Tohoku J. Exp. Med., 2023, **259**, 273-284

LILRB4/gp49B Co-Localizes with Integrin via Fibronectin at Focal Adhesion Sites on Mast Cells

Shotaro Miyamoto,[1] Takumi Chiba,[1] So Itoi,[1] Mei-Tzu Su[1] and Toshiyuki Takai[1]

[1]Department of Experimental Immunology, Institute of Development, Aging and Cancer, Tohoku University, Sendai, Miyagi, Japan

Mast cells protect a host from invasion by infectious agents and environmental allergens through activation of innate and adaptive immune receptors, their excessive activation being tightly regulated by inhibitory receptors, such as leukocyte immunoglobulin-like receptor (LILR)B4 (gp49B in mice). However, the regulatory mechanism of LILRB4/gp49B expressed on mast cells remains to be clarified in relation to their recently identified ligand, fibronectin (FN), a direct activator of integrins and an indirect stimulator of high-affinity Fc receptor for IgE (FcεRI). Confocal microscopic analysis suggested that gp49B is spatially close to integrin β_1 on non-adhered bone marrow-derived mast cells (BMMCs). Their spatial relatedness increases further at robust focal adhesion sites on cells adhering to immobilized FN. However, the confocal fluorescence signal of the α subunit of FcεRI was found to be correlated to neither gp49B nor integrin β_1 on non-adherent and adherent BMMCs. Stimulation of FcεRI with an immobilized antigen caused FcεRIα signals to accumulate in an inside area surrounded by robust focal adhesion with a concomitant slight increase in the signal correlation of FcεRIα and integrin β_1, accompanied by a less significant increase of the FcεRIα and gp49 correlation. Thus, activating and inhibitory FN receptors integrin and gp49B, respectively, were co-localized via FN at robust focal adhesion sites on BMMCs, while FcεRI was not close to gp49B spatially.

Keywords: allergy; FcεRI; fibronectin; immune checkpoint; lipid raft
Tohoku J. Exp. Med., 2023 April, **259** (4), 273-284.
doi: 10.1620/tjem.2023.J001

Introduction

Leukocyte immunoglobulin-like receptor (LILR)B4 (also known as ILT3/CD85k in humans and gp49B in mice) was initially identified as an inhibitory-type receptor expressed on murine mast cells (Castells et al. 1994; Katz et al. 1996), and later it was found to be expressed on various murine myeloid-lineage cells, such as uterine macrophages (Matsumoto et al. 2001), neutrophils (Zhou et al. 2003), and conventional dendritic cells (Kasai et al. 2008) and B-lineage cells, including murine marginal zone B cells (Fukao et al. 2014) and plasmablasts/plasma cells from humans and mice (Inui et al. 2016; Wong et al. 2019). LILRB4/gp49B is also expressed on murine natural killer cells (Wang et al. 1997), and activated T cells from humans and mice (Sharma et al. 2021).

Initially, gp49 was defined as a 49-kDa cell surface glycoprotein preferentially expressed on mouse IL-3-dependent bone marrow-derived mast cells (BMMCs), and later, molecular cloning studies identified two isoforms, a non-inhibitory-type gp49A and a supposed inhibitory-type, membrane-bound gp49B (Castells et al. 1994). Interestingly, it was shown that the interaction between gp49B and integrin $\alpha_v\beta_3$ inhibits IgE-mediated BMMC activation *in vitro*, suggesting the gp49B isoform is an inhibitory receptor that binds to integrin $\alpha_v\beta_3$ (Castells et al. 2001). Likewise in animal models of inflammation, gp49B deficiency is associated with increased cytokine and chemokine production, and the severity of proliferative synovitis induced by anti-type II collagen antibodies (Zhou et al. 2005). It was also suggested that gp49B on neutrophils plays a regulatory role in lipopolysaccharide-induced intravascular neutrophil adhesion and microangiopathy (Zhou et al. 2003). In addition, in tumor-bearing mouse models, anti-LILRB4/gp49B antibody administration could release LILRB4/gp49B-mediated, attenuated anti-tumor immunity,

Received October 13, 2022; revised and accepted January 2, 2023; J-STAGE Advance online publication January 13, 2023
Correspondence: Toshiyuki Takai, Department of Experimental Immunology, Institute of Development, Aging and Cancer, Tohoku University, 4-1 Seiryo-machi, Aoba-ku, Sendai, Miyagi 980-8575, Japan.
e-mail: toshiyuki.takai.b8@tohoku.ac.jp

and thus LILRB4 is a potential target for immunotherapy for solid tumors (Sharma et al. 2021; Paavola et al. 2021; Su et al. 2022) and acute myeloid leukemia (Deng et al. 2018). Therefore, understanding of the mode of function of LILRB4/gp49B and their ligand(s) in immunity is important to understand how the receptor-ligand interaction attenuates various cells in the immune system as a myeloid immune checkpoint.

In addition to the proposed ligand for murine gp49B, integrin $\alpha_v\beta_3$ (Castells et al. 2001; Katz 2007), several groups have recently reported ligand proteins for human LILRB4 (Xu et al. 2018; Deng et al. 2018; Su et al. 2021; Paavola et al. 2021). These include the activated lymphocyte cell adhesion molecule (ALCAM or CD166), an activation marker of T cells (Xu et al. 2018), and apolipoprotein E in humans (Deng et al. 2018). Importantly, the reported human LILRB4 ligands are not shared by murine gp49B (Xu et al. 2018; Deng et al. 2018). On the other hand, we found that both human LILRB4 and murine gp49B bind to fibronectin (FN) (Su et al. 2021). Furthermore, we found that the N-terminal 30 kDa domain of FN (FN30) contains a major, but not the sole, binding site. Blockade of FN30 binding to gp49B *in vivo* was shown to be effective in reducing IgG anti-double stranded DNA autoantibodies and in ameliorating glomerulonephritis in BXSB/*Yaa* lupus model mice, suggesting a role of LILRB4/gp49B-FN in autoimmune pathogenicity (Su et al. 2021) in addition to its pathogenic role in tumors. Others also reported FN is a ligand for human LILRB4 (Paavola et al. 2021). These findings suggested that FN is an intrinsic pathophysiologic ligand common to both human and mouse LILRB4/gp49B.

Generally, receptors for FN are known to be a group of classical FN-binding integrins, such as $\alpha_5\beta_1$, $\alpha_v\beta_1$, and $\alpha_v\beta_3$, some of which are expressed ubiquitously on cells, and $\alpha_{IIb}\beta_3$ mainly on platelets (Plow et al. 2000). Upon activation, these FN-binding integrins become associated with actin filaments intracellularly, and thus are related to cell activation and dynamics such as adhesion and migration. These integrins bind to the RGDS sequence (RGD motif) located in FN type III repeat 10 ($FNIII_{10}$), which is in the middle of a 220-250 kDa FN molecule (Plow et al. 2000; Pankov and Yamada 2002; Barczyk et al. 2010) (Fig. 1). On the other hand, FN30 is in the N terminal and thus is apart from the RGD motif. Given that FN is the common ligand for both inhibitory receptors LILRB4/gp49B and cell activating-type receptor integrin, it is tempting to determine the modes of LILRB4/gp49B- and integrin-mediated regulation in mast cells. Interestingly, FN in the extracellular matrix is considered to be an important regulator of mast cells (van Vugt et al. 1996; Houtman et al. 2001). It is reported that IgE triggers the adhesion of BMMCs and connective tissue mast cells to FN. This is mediated by increased avidity of integrin $\alpha_5\beta_1$ (also known as very late antigen 5 or VLA-5). FN was suggested to act synergistically with IgE to prolong intracellular phosphorylation events, and to enhance IgE-induced inflammatory cytokine production and BMMC survival (Lam et al. 2003). Thus, IgE and its high-affinity Fc receptor, FcεRI, could mediate an activation signal that stimulates integrin $\alpha_5\beta_1$ in mast cells, and *vice versa*. These observations indicate the possible formation of supramolecular activation clusters (SMACs) composed of integrin $\alpha_5\beta_1$, FcεRI, and FN, and of focal adhesion complexes harboring signaling molecules such as focal adhesion kinase as the most upstream ones (Houtman et al. 2001) (Fig. 1).

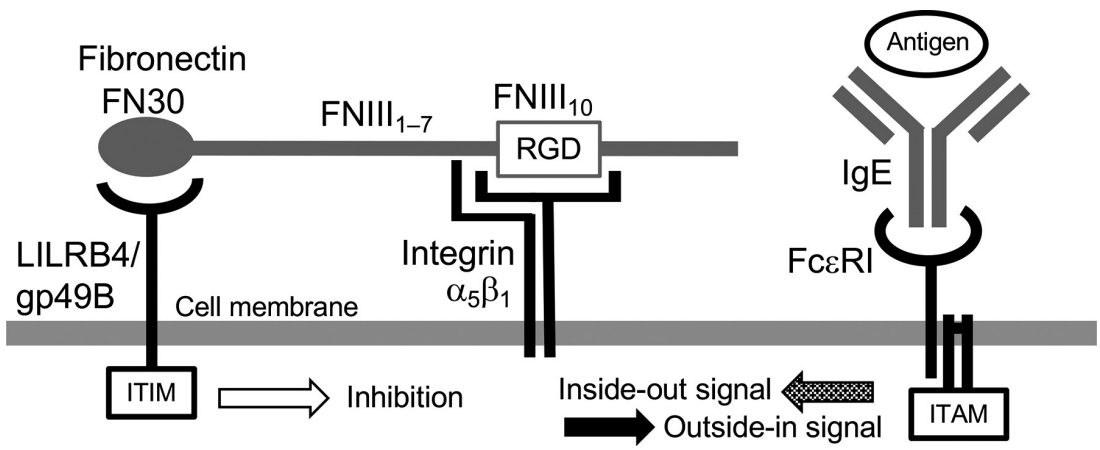

Fig. 1. Hypothetical structure of the LILRB4/gp49B-FN-integrin trimeric complex with a supposed interaction to FcεRI. Our hypothetical view of the potential communication between LILRB4/gp49B-integrin $\alpha_5\beta_1$ and the high-affinity Fc receptor for IgE (FcεRI) on mast cells. FN binding induces integrin $\alpha_5\beta_1$ activation leading to actin reorganization and a pro-inflammatory signal. LILRB4/gp49B is a negative regulator of the integrin-mediated activation via binding to the shared ligand, FN. On the other hand, FcεRI and integrin $\alpha_5\beta_1$ can communicate with each other via formation of supramolecular activation complexes (SMACs) on the cell surface. FN30, fibronectin N-terminal 30-kDa domain, a major site for LILRB4/gp49B binding; FNIII, fibronectin type III repeat; RGD, Arg-Gly-Asp, a major amino acid sequence for integrin binding; ITAM, immunoreceptor tyrosine-based activation motif; ITIM, immunoreceptor tyrosine-based inhibitory motif.

Since the SMAC formation of integrin $\alpha_5\beta_1$, FcεRI, and FN was suggested in FN-activated mast cells, and FN is the common ligand for both integrin $\alpha_5\beta_1$ and LILRB4/gp49B, we were interested in examining the relationship among integrin $\alpha_5\beta_1$, LILRB4/gp49B, FN, and FcεRI on FN-activated mast cells. Our hypothesis is that the LILRB4/gp49B-FN-integrin trimeric complex could have some relation to FcεRI on IgE-mediated, activated mast cells (Fig. 1). Supporting this in part, we recently showed the formation of the LILRB4/gp49B-FN-integrin trimeric complex on human monocytic cell line THP-1 and murine macrophages (Itoi et al. 2022), and the close spatial relationship between integrin and gp49B on murine bone marrow-derived dendritic cells (Takahashi et al. 2022). In this study we examined the feasibility of our hypothetical view by confocal microscopy.

Methods

Reagents and antibodies

FN from human plasma was purchased from Sigma-Aldrich (St. Louis, MO, USA). We used the following non-labeled or labeled antibodies: AlexaFluor546-conjugated anti-gp49 (#53584AF546) from Santa Cruz Biotechnology (Dallas, TX, USA); APC-labeled anti-c-kit (2B8, BioLegend, San Diego, CA, USA); PE-labeled anti-FcεRIα (MAR-1, eBioscience, San Diego, CA, USA); Alexa 647-anti-mouse integrin β_1 (MB1.2, Sigma-Aldrich); β_2 (M18/2, BioLegend); Alexa647-anti-mouse integrin β_3 (2C9.G2, BioLegend); Alexa 647-labeled anti-mouse integrin α_2 (HMα2, BioLegend); Alexa 488-labeled anti-mouse integrin α_4 (R1-2, BioLegend); APC-labeled anti-mouse integrin αM (M1/70, BioLegend); PE-labeled anti-mouse interin α_{IIb} (MWReg30, BioLegend); PE-labeled anti-mouse integrin α_5 (HMa5-1, BioLegend); Alexa488-labeled anti-FN30 made in house; non-labeled anti-FN module III (clone 14, Thermo Fisher Scientific, Waltham, MA, USA), rabbit polyclonal anti-FN N-terminal FN1 IgG (N1N2, GeneTex Inc., Irvine, CA, USA); rabbit polyclonal anti-whole FN IgG (F3648, Sigma-Aldrich); Alexa488-labeled anti-rabbit IgG; Alexa 647-labeled anti-mouse H2-K^b/D^b (28-8-6, BioLegend); and Alexa 546-labeled anti-mouse β_2 microglobulin (S19.8, BD Biosciences, Franklin Lakes, NJ, USA). Anti-FN30 mAbs (#5) were established in our laboratory. H1.1 (anti-gp49 IgG mAb, derived from Armenian hamsters) hybridoma cells were kindly provided by Dr. Wayne M. Yokoyama (Wang et al. 2000).

Mice

C57BL/6 mice were purchased from CLEA Japan (Tokyo, Japan). gp49B-deficient C57BL/6 mice were generated in house as described previously (Kasai et al. 2008). All mice were maintained and bred in the animal facility of the Institute of Development, Aging and Cancer, Tohoku University, under specific pathogen-free conditions, and used for experiments at 8-9 weeks old. All animal protocols were reviewed and approved by the Animal Studies Committee of Tohoku University.

In vitro culture of bone marrow-derived mast cells (BMMCs) and a mast cell line, SVMC

BMMCs were prepared as described previously (Kanehira et al. 2006). Briefly, bone marrow cells were prepared from mouse femur and tibial bones, and red blood cells were lysed with a 155 mM NH_4Cl, 10 mM $KHCO_3$, and 0.1 mM EDTA solution. For preparing BMMCs, bone marrow cells were cultured in RPMI1640 (Sigma-Aldrich) comprising heat-inactivated fetal bovine serum (FBS, Biowest, Nuaille, FR, USA), 1 mM sodium pyruvate, 50 μM 2-mercaptoethanol, 100 U/ml penicillin (Sigma-Aldrich), 100 μg/ml streptomycin (Sigma-Aldrich), and 5 ng/ml recombinant IL-3 (R&D Systems, Inc., Minneapolis, MN, USA) at 37˚C under a humidified atmosphere containing 5% CO_2. Non-adherent cells were transferred every 6-7 days to new culture flasks at a density of 3×10^5 cells/ml over a 4- to 5-week culture period. Floating cells were recovered after swirling the contents of the culture bottle and used for further experiments as BMMCs.

Flow cytometry (FCM) analysis and cell sorting

Cells were stained for 1 h on ice in phosphate-buffered saline (PBS) containing 2% FBS with fluorochrome-labeled antibodies. Prior to this, all samples were treated with non-conjugated anti-CD16/CD32 (clone 2.4G2) for 30 min to prevent non-specific antibody binding due to the Fcγ receptors. Samples were analyzed and sorted using FACSAria III (BD Biosciences). Data were collected using FACS Diva software and analyzed using FlowJo software (Tree Star).

Confocal laser-scanning microscopic analysis

The distribution of cell surface proteins gp49, integrin β_1, and FcεRIα was assessed by confocal microscopy. Cells were plated onto glass-bottom dishes [Matsunami, Kishiwada, Japan; poly-lysine coated, dish diameter 35 mm, glass diameter 14 mm, glass thickness No.1S/1.5 (0.16-0.19 mm), and #D11131H]. Cells were fixed with 1% paraformaldehyde (PFA) for 30 min on ice and then washed three times with a washing solution [1% bovine serum albumin (BSA) in PBS]. The fixed cells were then stained with the antibodies of interest, i.e., AlexaFluor546-conjugated anti-gp49 (#53584AF546; Santa Cruz), AlexaFluor647-conjugated anti-integrin β_1 (MAB1997-AF647; ThermoFisher Scientific), or FITC-conjugated anti-FcεRIα (MAR-1, BioLegend). After thorough washing, the cells were mounted using SlowFade-Gold Antifade reagent (ThermoFisher Scientific) and then examined at 2-D under a Leica SP8 confocal microscope system. Isolation of peritoneal residential macrophages was as described previously (Itoi et al. 2022).

Evaluation of Pearson's correlation coefficients between fluorescence signals of cell-surface molecules

Correlation coefficient r between two sets of observed parameters, namely the fluorescence signals of gp49, integrin β_1, and FcεRIα in this study, was evaluated as described for Pearson's correlation analysis (Adler and Parmryd 2010). Briefly, each signal profile of a cell contour was analyzed with the software with a Leica SP8, the r value being calculated. The r values were obtained for over 10-34 cells randomly selected in the captured images and are illustrated as a graph. Mean r values were interpreted according to the following criteria: $r = -1$, perfect negative linear relationship; $-1 < r \leq -0.70$, strong negative linear relationship; $-0.7 < r \leq -0.4$, negative relationship; $-0.4 < r \leq -0.2$, weak negative linear relationship; $-0.2 < r \leq +0.20$, no significant relationship; $+0.2 < r \leq +0.4$, weak positive relationship; $+0.4 < r \leq +0.7$, positive linear relationship; $+0.7 < r < +1$, strong positive linear relationship; and $r = +1$, perfect positive linear relationship. We considered $r > +0.2$ as a positive correlation.

Adherence of BMMCs to immobilized fibronectin (FN)

For preparation of immobilized FN, a human FN solution was diluted to 10 µg/ml with PBS and then added to a 96-well culture plate, followed by incubation for 16 h at 37˚C, and then the plate was washed twice with PBS before use. BMMCs were plated into the FN-coated or noncoated wells at 2.0×10^5 cells/well, followed by incubation at 37˚C for different periods.

Stimulation of FcεRI on BMMCs with anti-trinitrophenyl (TNP) IgE and TNP-ovalbumin (OVA)

A TNP-OVA-coated dish was prepared as follows. 150 µl of either 10 µg/ml FN or 10 µg/ml TNP-OVA or a mixture of them was added to a glass-bottom dish for confocal analysis, followed by incubation for 16 h at 37˚C, and then the plate was washed twice with PBS before use. BMMCs were sensitized with 5 µg/ml anti-TNP IgE for 1 h at 37˚C, treated for FcγR blocking with 2.4G2 mAb, and then washed with PBS. 2.0×10^4 cells were plated onto FN-, TNP-OVA-, FN plus TNP-OVA-coated plates, followed by incubation for 40 min at 37˚C and then confocal analysis.

Statistical analysis

Statistical analyses were carried out using GraphPad Prism® 6 (Version 6.0; GraphPad Software, San Diego, CA, USA). Data are presented when appropriate as means ± SD. Data were compared for statistical differences as to Pearson's correlation coefficients with the two-tailed paired Student's t-test. We considered $p < 0.05$ as being statistically significant.

Results

Expression profiles of integrins, FN, and gp49B on bone marrow-derived mast cells (BMMCs)

We initially checked the expression of FcεRI and c-kit as typical mast cell markers on BMMCs, and verified gp49B expression on the surface (Fig. 2). Flow cytometric analysis confirmed that the BMMCs were positive for the FcεRI α subunit and c-kit as well as for surface gp49. On BMMCs, dominant expression of gp49B over the gp49A isoform was observed on use of gp49B-deficient BMMCs (Fig. 2A). As a reference, we also checked a murine mast cell line, SVMC, in which FcεRIα, c-kit, and gp49 were positive on the cell surface (Fig. 2B).

We then checked the expression of a ubiquitous FN-binding integrin, $\alpha_5\beta_1$, and other integrin α and β subunits that may contribute to FN binding, namely α_2, α_4, α_6, αM, α_{IIb}, α_v, β_2, and β_3 (Fig. 3A, B), as well as FN (Fig. 3C) on the BMMC surface. Flow cytometric analysis of integrin subunits, and FN30 and FN type III repeat 7-9 ($FNIII_{7\text{-}9}$, see Fig. 1) expression revealed that BMMCs were positive for integrin α_2, α_4, α_5, α_6, α_v, α_{IIb}, β_1, β_2, β_3, and $FNIII_{7\text{-}9}$, but negative for integrin α_M and FN30 (Fig. 3A-C). Additional flow cytometric (Fig. 3D) and confocal microscopic (Fig. 3E) analyses of the FN N-terminal portion again indicated that the epitope was hardly detected on BMMCs compared to a positive control, HepG2 cells (Fig. 3D), and peritoneal macrophages (Fig. 3E). SVMCs were positive for surface integrins α_5, α_6, β_1, β_2, and β_3, but negative for other integrin α chains, FN30 and FNIII (Fig. 3A-D). Based on these results, we concluded that major FN-binding integrin $\alpha_5\beta_1$ (VLA-5), and various other FN-cognate integrins, such as $\alpha_6\beta_1$, $\alpha_v\beta_3$ and $\alpha_{IIb}\beta_3$, are expressed on the surface of BMMCs, while $\alpha_5\beta_1$ and $\alpha_6\beta_1$ are FN-binding integrins expressed on SVMCs. FN, except for its N-terminal portion, was positive on BMMCs. FN was totally negative on SVMCs. We concluded at this stage that FN is tethered on BMMCs by the cognate integrin, albeit the N-terminal FN30 epitope expression was only marginal on the cells.

Correlation of gp49, integrin β_1, and FcεRIα signals on non-adhered BMMCs

We examined the fluorescence signals of gp49, the integrin β_1 subunit, and the FcεRIα chain on the surface of non-adhered, floating BMMCs by confocal microscopy. To this end, firstly we analyzed the signal correlation between the MHC class I α chain and β_2 microglobulin (β_2m) on the BMMCs as a positive control (Fig. 4A). The confocal microscopic signals for MHC class I α and β_2m on cell contour lines were also analyzed and are illustrated as histograms, which showed remarkably matched profiles (Fig. 4B). Next, we examined the signals of FcεRIα, gp49, and integrin β_1 on the surface of floating, non-adhered BMMCs. The fluorescence signal profile was again grossly ring-like for FcεRIα, gp49 and integrin β_1 like for MHC class I α and β_2m (Fig. 4C), and the signal correlations on contours were

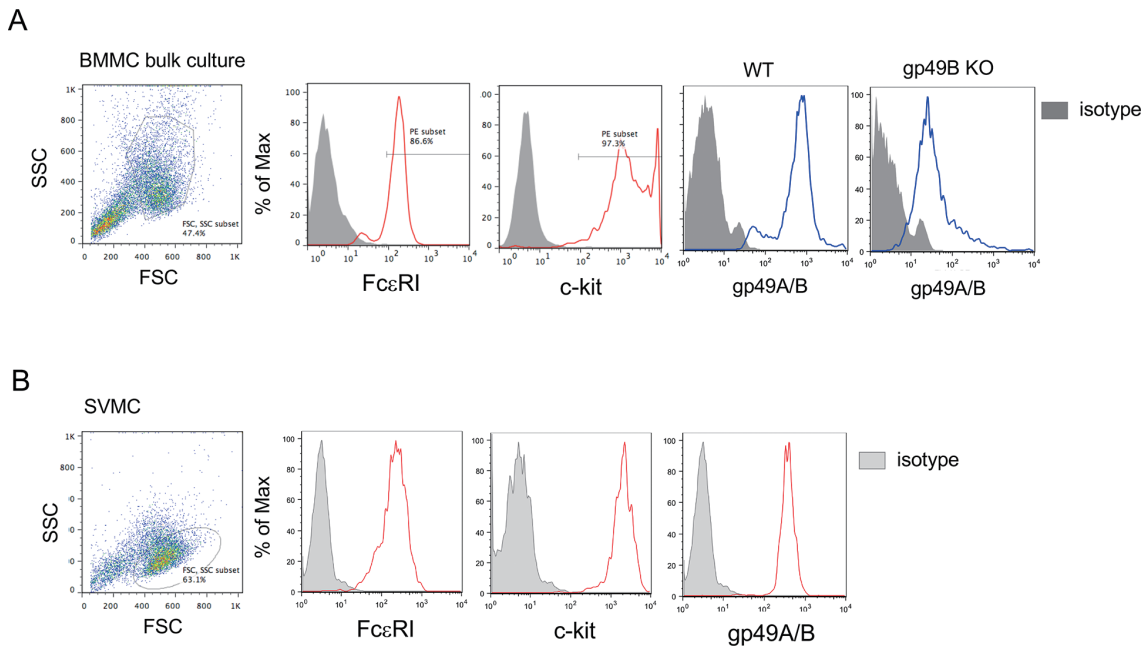

Fig. 2. Characterization of bone marrow-derived mast cells (BMMCs) and a mast cell line, SVMC. (A) Murine BMMCs prepared as described under *Materials and Methods* were gated, and then analyzed for their cell-surface expression of FcεRI, c-kit, and gp49 by flow cytometry. Analysis of gp49A/B expression on BMMCs was also performed for cells from gp49B-deficient mice. The gp49A expression level (rightmost) was low, suggesting that gp49B expression is dominant on the surface of BMMCs. (B) Similar analysis was performed for SVMCs.

analyzed. Correlation histograms of these three fluorochromes are also shown (Fig. 4D).

The signal correlations between molecules along a contour line were calculated as Pearson's correlation (r) values, as shown in Fig. 4E. We found that the correlation for a positive control was reasonably high, which was judged as a positive linear relationship (r = 0.528 ± 0.052, mean ± SD, n = 3). We observed a weak positive relationship for gp49 and integrin β_1 (r = 0.296 ± 0.096, mean ± SD, n = 14). These results suggested that gp49 and integrin β_1 are spatially close on the cell membrane like on bone marrow-derived cultured dendritic cells (Takahashi et al. 2022). However, the signal correlation of both FcεRIα-gp49 and FcεRIα-integrin β_1 was not significant (r = 0.175 ± 0.073 and 0.159 ± 0.072, respectively, mean ± SD, n = 14), suggesting that the either FcεRIα and gp49 or integrin β_1 are mutually apart on the surface of non-adhered BMMCs. Collectively, these results supported a spatially close relationship between gp49B and integrin β_1 via FN on the surface of BMMCs. Interestingly, however, the localization of gp49B-integrin and that of FcεRIα did not correlate on the cell surface of non-adhered BMMCs.

Correlation of gp49, integrin β_1, and FcεRIα signals at focal adhesion sites on BMMCs adhered to an FN-coated dish

We next examined the fluorescence signals of gp49, integrin β_1, and FcεRIα at the focal adhesion sites on BMMCs adhering to a FN-coated dish. Like non-adhered BMMCs, the positive control MHC class Iα and β_2m signals correlated well (Fig. 5A, B). We also checked the correlation between the signals for β_2m and integrin β_1, a supposedly negative combination, and found there was no significant correlation (Fig. 5C, D). The fluorescence signals of FcεRIα appeared as relatively sharp dots, and those of gp49 and integrin β_1 were mainly distributed in a similar area, corresponding to typical ring-like focal adhesion (Fig. 5E). The correlation histogram of each pair of these three fluorochromes on contour lines obtained for such robust focal adhesion areas (Fig. 5E, rightmost) was analyzed (Fig. 5F-H). We observed a positive relationship for the Pearson's correlation for gp49 and integrin β_1 (Fig. 5I), and it was found to be more elevated than that for BMMCs adhered to a non-coated dish (Fig. 5J). The signal correlations of both FcεRIα-gp49 and FcεRIα-integrin β_1 were not significant (Fig. 5F, H, I), suggesting that the compartments of FcεRIα and gp49-integrin β_1 do not overlap significantly also in robust focal adhesion areas. Collectively, these results supported a spatially close relationship between gp49B and integrin β_1 via immobilized FN as well as cell-intrinsic FN at robust focal adhesion sites on BMMCs. However, the compartment of gp49B-FN-integrin β_1 and that of FcεRIα might be apart from each other also at robust focal adhesion sites on BMMCs. In addition, we cannot rule out the involvement of the effect of outside-in/inside-out signals on the closer relationship between gp49B and integrin β_1 in the presence of FN.

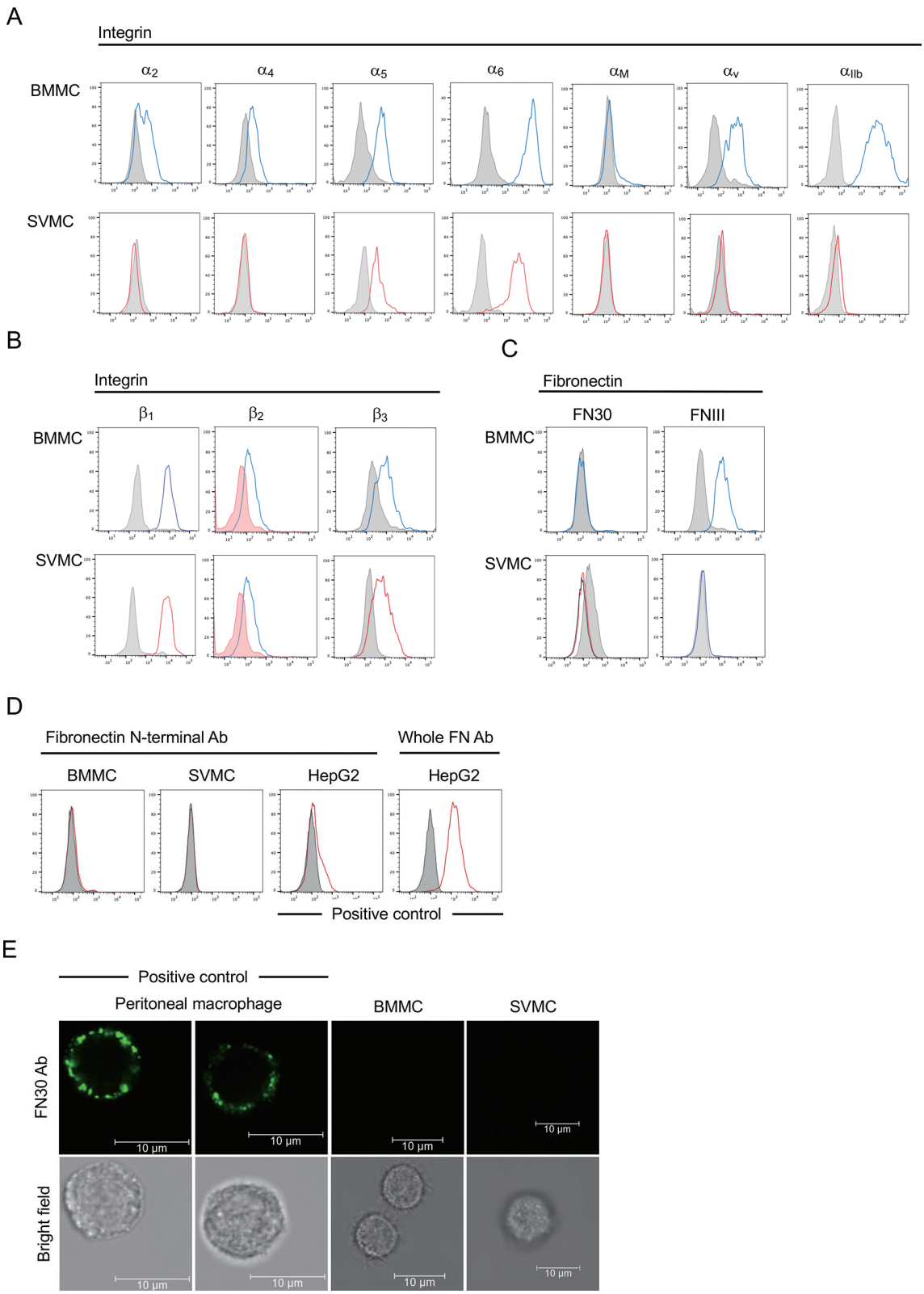

Fig. 3. Cell-surface expression profiles of integrin α and β chains, and fibronectin (FN) on BMMCs.
BMMCs were analyzed for their cell-surface expression of the integrin α (A) and β (B) chains, and the FN N-terminal 30 kDa domain (FN30) and FN module III (FNIII) (C) by flow cytometry. Gray areas indicate an isotype control. Black line for FN30 expression on SVMCs (C, lower left) indicates no stain control. FNIII but not FN30 expression was reproducibly observed on BMMCs. N-terminal FN expression was scarcely detected on BMMCs with another specific antibody (D). Confocal microscopy detects FN30 on peritoneal residential macrophages but neither BMMCs nor SVMCs (E).

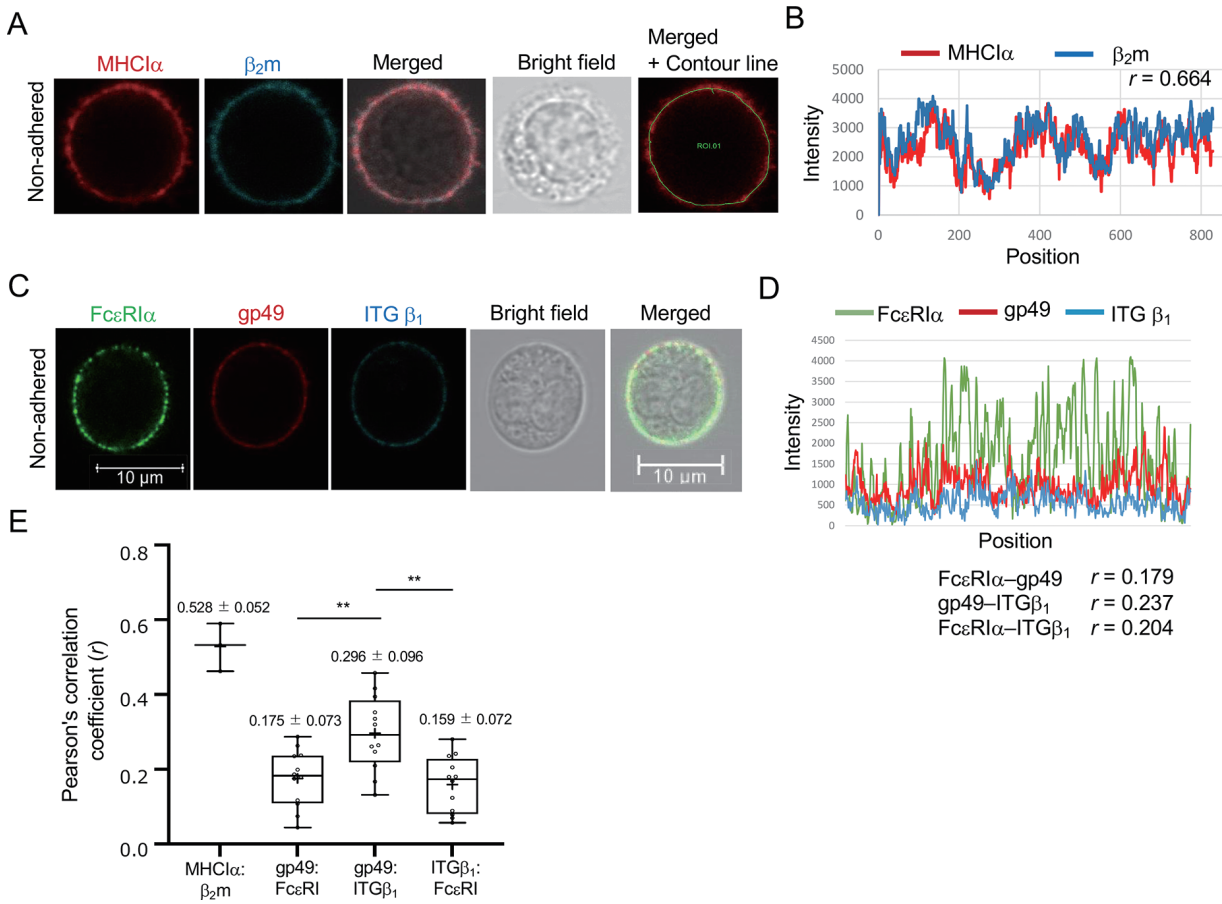

Fig. 4. Confocal microscopic and correlation analyses of fluorescence signals of gp49, integrin β_1, and FcεRIα on the cell surface of non-adhered BMMCs.
(A, B) Confocal microscopic images of cell surface MHC class I α chain and β_2 microglobulin (β_2m) as positive controls for correlation analysis (A), and correlation histograms of the signals (B) measured on the contour line set arbitrarily on the merged image (A, rightmost). (C, D) Confocal microscopic images of cell surface FcεRI α chain, gp49, and integrin β_1 (C), and correlation histograms of their signals (D) measured on the contour line set arbitrarily on the merged image. (E) Pearson's correlations of the MHC class I α and β_2m signals, and those of FcεRIα, gp49, and integrin β_1 were analyzed. In the box plot, the upper and lower whiskers denote the maximum and minimum values of the data set, respectively. The box indicates the area between the upper and lower quartiles, with a horizontal line indicating the median of all data and X as the mean. Correlation values are expressed as means ± SD (two-tailed paired *t*-test; n = 3 for positive control and n = 14 for others). $^{**}p < 0.01$.

Correlation of gp49, integrin β_1, and FcεRIα signals at focal adhesion sites on IgE-stimulated BMMCs adhered to an FN plus antigen-coated dish

IgE/FcεRI trigger the adhesion of BMMCs to FN, which is mediated by increased avidity of integrin $\alpha_5\beta_1$ as to FN via an inside-out signal, and *vice versa* via an outside-in signal (Fig. 1). To determine how FcεRI stimulation could influence gp49B and integrin co-localization, we analyzed the fluorescence signals of gp49, integrin β_1, and anti-TNP IgE-sensitized FcεRIα in the focal adhesion plane of BMMCs adhered to an FN-coated dish in the presence or absence of an antigen, TNP-OVA. We observed that the antigen stimulation induced membrane ruffling in many cells, plausibly due to degranulation, so we chose cells without severe ruffling for our confocal analysis. In such less ruffled cells, we found that the fluorescence signal of FcεRIα in the focal adhesion plane tended to be centered on an inside region rather than the outer area of adhesion (Fig. 6A-D, green), while the distribution of the gp49 signal mostly remained in the outer area (Fig. 6A-D, red). On the other hand, the integrin β_1 signal was found to be partly distributed also in the inside region (Fig. 6A-D, blue). These signal profiles were grossly similar in the cells adhered to a TNP-OVA-coated dish with or without FN, suggesting that the distribution shift of integrin β_1 as well as FcεRIα was not tightly dependent on FN but TNP-OVA.

The correlation histograms of each pair of these three signals on arbitrarily-drawn straight lines across the whole cells, contour lines, and inside lines were analyzed (Fig. 6E). We again observed a positive relationship for the Pearson's correlation for gp49 and integrin β_1 on every type of line, even in the presence of TNP-OVA. In the absence of FN, however, this correlation between gp49-integrin β_1 on every line was less evident than that in the presence of

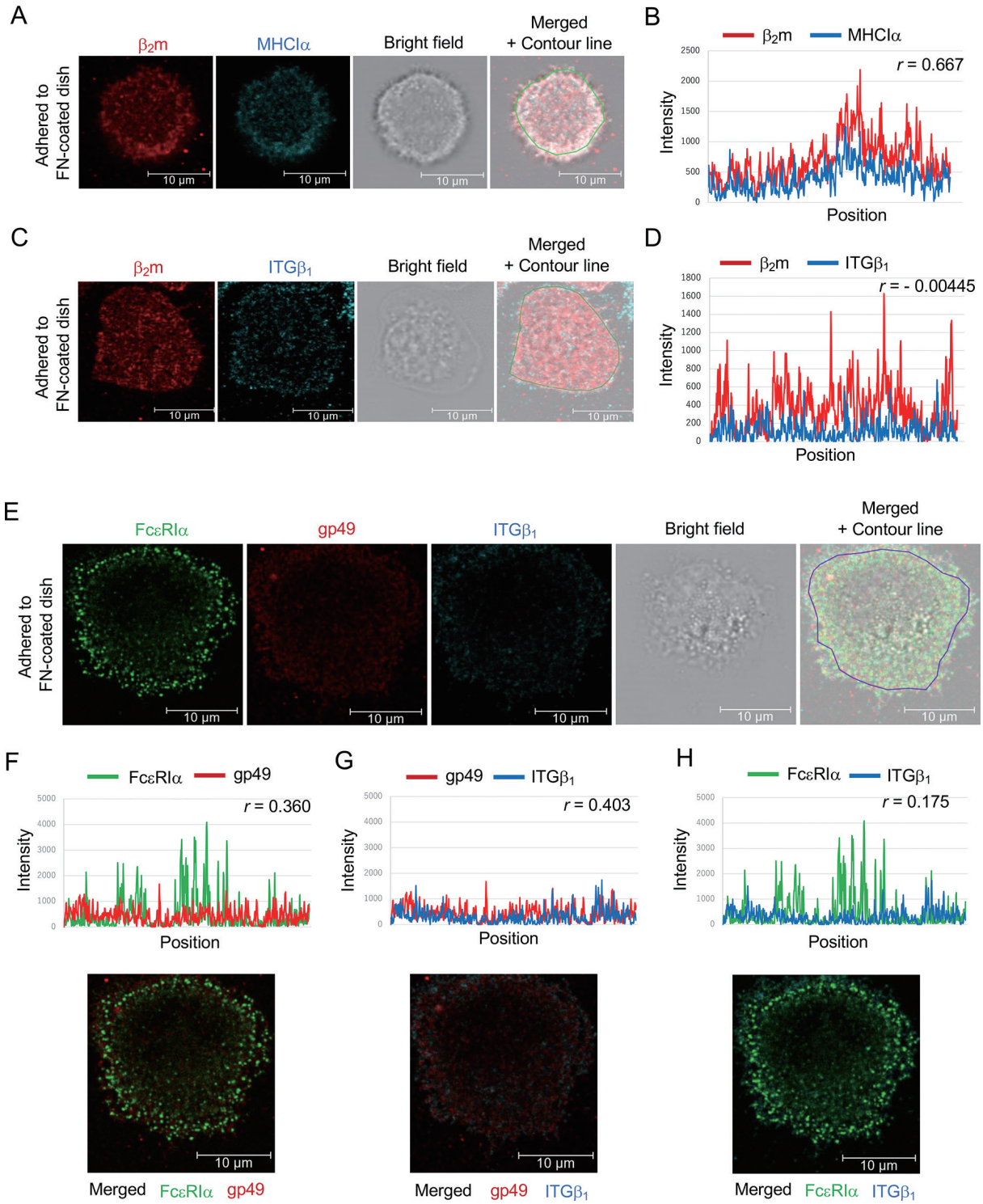

FN as expected. Signal correlation of FcεRIα-gp49 was not evident on every line in the absence of FN (Fig. 6E, upper), or on the across and contour lines in the presence of FN (Fig. 6E, lower left and middle), but it was markedly increased on the inside line in the presence of TNP-OVA and FN, for which the correlation was almost a significant level (Fig. 6E, lower right, $r = 0.198 \pm 0.181$). The FcεRIα-integrin β_1 signal correlation tended to be increased to a significant level, particularly on inside lines in the presence of FN (Fig. 6E, lower right, $r = 0.300 \pm 0.167$). Collectively, these results supported the notion that integrin $\alpha_5\beta_1$ becomes close to FcεRI upon antigen stimulation in the presence of FN (Houtman et al. 2001). Interestingly, gp49B kept a spatially close relationship to integrin β_1 but not to FcεRI in robust focal adhesion areas even after antigen/IgE-mediated FcεRI activation.

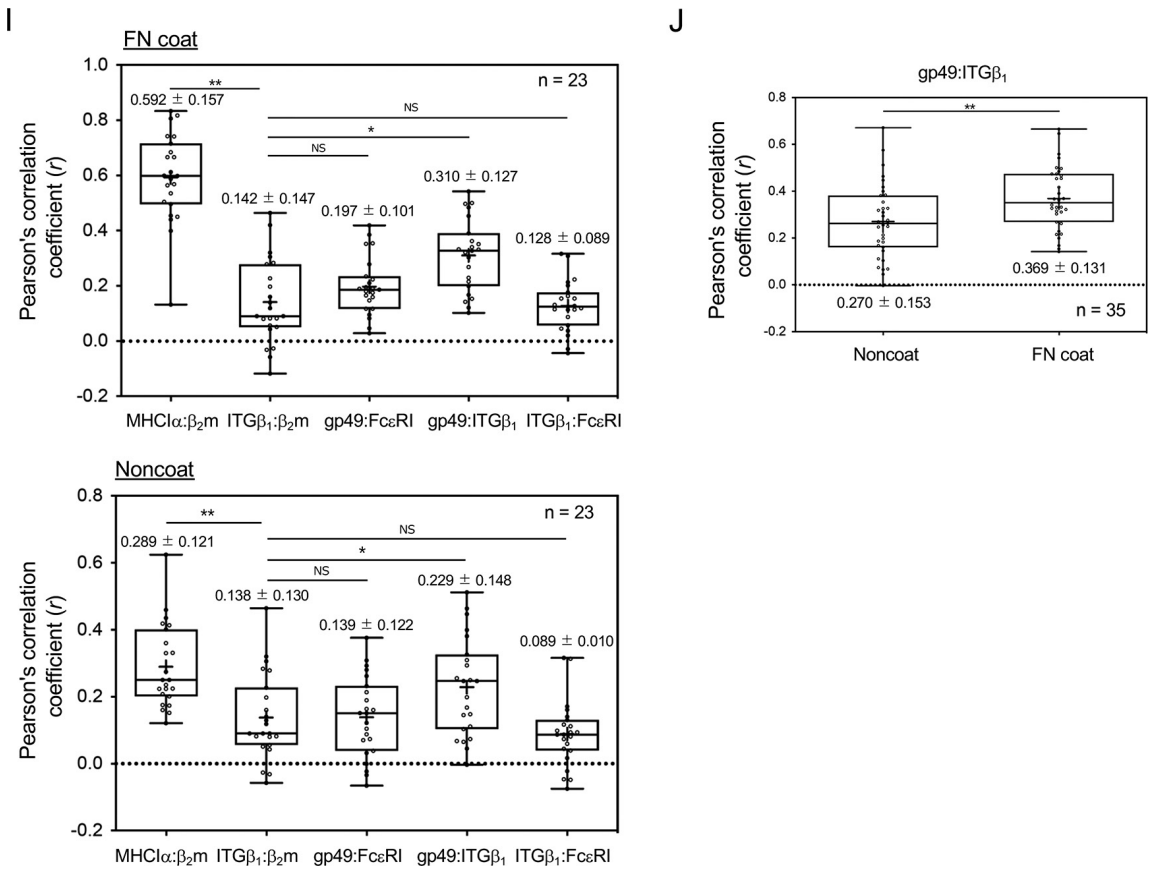

Fig. 5. Confocal microscopic and correlation analyses of fluorescence signals of FcεRIα, gp49, and integrin β_1 on the cell surface of BMMCs adhered to an FN-coated dish.
(A-D) Confocal microscopic images of β_2 microglobulin (β_2m) and MHC class I α chain (A), and a correlation histogram (B) for a positive control, and ones for β_2m and integrin β_1 for a negative control (C, D) captured on the focal adhesion planes of BMMCs adhered to an FN-coated dish. Rounded lines were set arbitrarily near the outermost areas, and the signal correlations are depicted as correlation histograms (A, C, rightmost). (E-H) Confocal microscopic images of cell surface FcεRI α chain, gp49, and integrin β_1 (E), and correlation histograms of their signals (F-H) measured on the rounded line set arbitrarily near the outermost areas of a merged image (E, rightmost). (I) Pearson's correlations of the MHC class I α and β_2m signals, and those of FcεRIα, gp49, and integrin β_1 were analyzed. In the box plot, the upper and lower whiskers denote the maximum and minimum values of the data set, respectively. The box indicates the area between the upper and lower quartiles, with a horizontal line indicating the median of all data and + as the mean. Correlation values are expressed as means ± SD (two-tailed paired *t*-test; n = 23). $*p < 0.05$, $**p < 0.01$. NS, not significant.
(J) Comparison of the Pearson's correlations of the gp49 and integrin β_1 signals in focal adhesion areas on BMMCs adhered to FN-coated and non-coated dishes. The box indicates as above. Correlation values are expressed as means ± SD (two-tailed paired *t*-test; n = 35). $**p < 0.01$.

Discussion

In this study, flow cytometric and confocal laser-scanning microscopic analyses of gp49, integrin β_1, and FcεRIα revealed that gp49B and integrin $\alpha_5\beta_1$ are spatially close via FN on the BMMC surface. gp49B-FN-integrin $\alpha_5\beta_1$ trimeric complex formation, on confocal microscopic analysis, was suggested to become more significant at focal adhesion sites upon cell adhesion to an FN-coated dish. We found that FcεRI was not spatially very close to either gp49B or integrin $\alpha_5\beta_1$ on non-adhered or adhered BMMCs, while activation of FcεRI made integrin $\alpha_5\beta_1$ become closer to FcεRI accumulating to the central area of adhesion surrounded by a ring-like, robust focal adhesion site in the presence of FN.

LILRB4/gp49B deficiency upregulates tyrosine phosphorylation of Syk but not FAK as an immediate downstream signaling event coupled to FN-induced integrin activation in macrophages and dendritic cells (Itoi et al. 2022; Takahashi et al. 2022). Our current observations on mast cells suggest that mast cells also could have an important regulatory system in which LILRB4/gp49B suppresses the FN-integrin-mediated pro-inflammatory signal. However, our preliminary studies on intracellular signaling of BMMCs indicated that Syk and FAK expression as well as the phosphorylation levels were much lower than those on macrophages and bone marrow-derived dendritic cells (data not shown). Thus, the functional rationale remains to be determined for close gp49B-integrin $\alpha_5\beta_1$ and more distal FcεRI as well as for a closer relationship among gp49B-

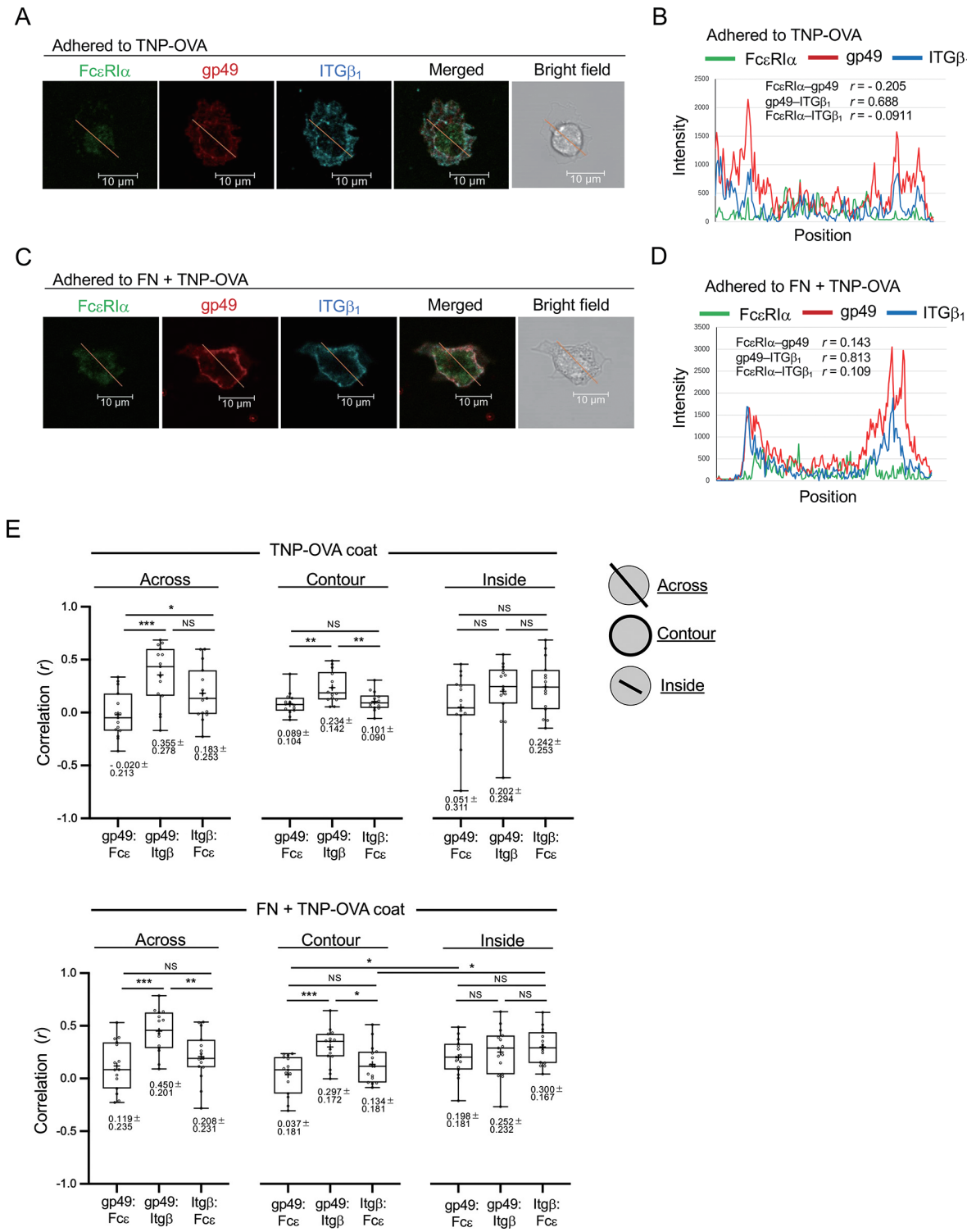

Fig. 6. Confocal microscopic and correlation analyses of fluorescence signals of FcεRIα, gp49, and integrin β_1 on the surface of FcεRI-activated BMMCs adhered to FN and antigen coated dishes.
(A-D) Confocal microscopic images of cell surface FcεRI α chain, gp49, and integrin β_1 of BMMCs adhered to dishes coated with TNP-OVA (A) or TNP-OVA and FN (C). BMMCs were pre-sensitized with anti-TNP IgE. Typical histograms of the three signals measured on a straight line set arbitrarily across a cell are shown (B, D). (E) Pearson's correlations of FcεRIα, gp49, and integrin β_1 were determined for those on three types of line: across a cell (left), contour of a cell (middle), and inside area of a cell (right), adhered to a TNP-OVA-coated dish (upper) or FN + TNP-OVA-coated dish (lower). In the box plot, the upper and lower whiskers denote the maximum and minimum values of the data set, respectively. The box indicates the area between the upper and lower quartiles, with a horizontal line indicating the median of all data and + as the mean. Correlation values are expressed as means ± SD (two-tailed paired *t*-test; n = 15). $*p < 0.05$, $**p < 0.01$, $***p < 0.001$. NS, not significant; TNP-OVA, 2,4,6-trinitrophenyl ovalbumin.

integrin and FcεRI in an inside area surrounded by robust focal adhesion upon FcεRI stimulation. It is plausible that mast cells in connective as well as mucosal tissues interact constitutively with the extracellular matrix containing FN. The effect of such a constitutive FN-LILRB4/gp49B interaction on homeostasis of tissue-resident mast cells will be our next subject of research.

In conclusion, our hypothetical view of the LILRB4/gp49B-FN-integrin trimeric complex (Fig. 1) is supported also for BMMCs like macrophages and dendritic cells reported previously (Itoi et al. 2022; Takahashi et al. 2022). LILRB4/gp49B should be counter-regulators of integrin. They could also be regulators for antigen/IgE/FcεRI-mediated activation of mast cells.

Acknowledgments

We thank W.M. Yokoyama (Washington University School of Medicine, St. Louis) for providing the H1.1 hybridoma, and N. Halewood for the English editing.

Funding was provided by a research grant from the Ministry of Education, Culture, Sports, Science and Technology of Japan (19H03484 to T.T.), and by JST SPRING (JPMJSP2114 to S.M.).

Conflict of Interest

The authors declare no conflict of interest.

References

Adler, J. & Parmryd, I. (2010) Quantifying colocalization by correlation: the Pearson correlation coefficient is superior to the Mander's overlap coefficient. *Cytometry A*, **77**, 733-742.

Barczyk, M., Carracedo, S. & Gullberg, D. (2010) Integrins. *Cell Tissue Res.*, **339**, 269-280.

Castells, M.C., Klickstein, L.B., Hassani, K., Cumplido, J.A., Lacouture, M.E., Austen, K.F. & Katz, H.R. (2001) gp49B1-alpha(v)beta3 interaction inhibits antigen-induced mast cell activation. *Nat. Immunol.*, **2**, 436-442.

Castells, M.C., Wu, X., Arm, J.P., Austen, K.F. & Katz, H.R. (1994) Cloning of the gp49B gene of the immunoglobulin superfamily and demonstration that one of its two products is an early-expressed mast cell surface protein originally described as gp49. *J. Biol. Chem.*, **269**, 8393-8401.

Deng, M., Gui, X., Kim, J., Xie, L., Chen, W., Li, Z., He, L., Chen, Y., Chen, H., Luo, W., Lu, Z., Xie, J., Churchill, H., Xu, Y., Zhou, Z., et al. (2018) LILRB4 signalling in leukaemia cells mediates T cell suppression and tumour infiltration. *Nature*, **562**, 605-609.

Fukao, S., Haniuda, K., Nojima, T., Takai, T. & Kitamura, D. (2014) gp49B-mediated negative regulation of antibody production by memory and marginal zone B cells. *J. Immunol.*, **193**, 635-644.

Houtman, R., Koster, A.S. & Nijkamp, F.P. (2001) Integrin VLA-5: modulator and activator of mast cells. *Clin. Exp. Allergy*, **31**, 817-822.

Inui, M., Sugahara-Tobinai, A., Fujii, H., Itoh-Nakadai, A., Fukuyama, H., Kurosaki, T., Ishii, T., Harigae, H. & Takai, T. (2016) Tolerogenic immunoreceptor ILT3/LILRB4 paradoxically marks pathogenic auto-antibody-producing plasmablasts and plasma cells in non-treated SLE. *Int. Immunol.*, **28**, 597-604.

Itoi, S., Takahashi, N., Saito, H., Miyata, Y., Su, M.T., Kezuka, D., Itagaki, F., Endo, S., Fujii, H., Harigae, H., Sakamoto, Y. & Takai, T. (2022) Myeloid immune checkpoint ILT3/LILRB4/gp49B can co-tether fibronectin with integrin on macrophages. *Int. Immunol.*, **34**, 435-444.

Kanehira, M., Kaifu, T., Maya, K., Kaji, M., Nakamura, A., Obinata, M. & Takai, T. (2006) Novel mast cell lines with enhanced proliferative and degranulative abilities established from temperature-sensitive SV40 large T antigen transgenic mice. *J. Biochem.*, **140**, 211-220.

Kasai, S., Inui, M., Nakamura, K., Kakizaki, Y., Endo, S., Nakamura, A., Ito, S. & Takai, T. (2008) A novel regulatory role of gp49B on dendritic cells in T-cell priming. *Eur. J. Immunol.*, **38**, 2426-2437.

Katz, H.R. (2007) Inhibition of pathologic inflammation by leukocyte Ig-like receptor B4 and related inhibitory receptors. *Immunol. Rev.*, **217**, 222-230.

Katz, H.R., Vivier, E., Castells, M.C., McCormick, M.J., Chambers, J.M. & Austen, K.F. (1996) Mouse mast cell gp49B1 contains two immunoreceptor tyrosine-based inhibition motifs and suppresses mast cell activation when coligated with the high-affinity Fc receptor for IgE. *Proc. Natl. Acad. Sci. U. S. A.*, **93**, 10809-10814.

Lam, V., Kalesnikoff, J., Lee, C.W., Hernandez-Hansen, V., Wilson, B.S., Oliver, J.M. & Krystal, G. (2003) IgE alone stimulates mast cell adhesion to fibronectin via pathways similar to those used by IgE + antigen but distinct from those used by Steel factor. *Blood*, **102**, 1405-1413.

Matsumoto, Y., Wang, L.L., Yokoyama, W.M. & Aso, T. (2001) Uterine macrophages express the gp49B inhibitory receptor in midgestation. *J. Immunol.*, **166**, 781-786.

Paavola, K.J., Roda, J.M., Lin, V.Y., Chen, P., O'Hollaren, K.P., Ventura, R., Crawley, S.C., Li, B., Chen, H.H., Malmersjo, S., Sharkov, N.A., Horner, G., Guo, W., Kutach, A.K., Mondal, K., et al. (2021) The fibronectin-ILT3 interaction functions as a stromal checkpoint that suppresses myeloid cells. *Cancer Immunol. Res.*, **9**, 1283-1297.

Pankov, R. & Yamada, K.M. (2002) Fibronectin at a glance. *J. Cell Sci.*, **115**, 3861-3863.

Plow, E.F., Haas, T.A., Zhang, L., Loftus, J. & Smith, J.W. (2000) Ligand binding to integrins. *J. Biol. Chem.*, **275**, 21785-21788.

Sharma, N., Atolagbe, O.T., Ge, Z. & Allison, J.P. (2021) LILRB4 suppresses immunity in solid tumors and is a potential target for immunotherapy. *J. Exp. Med.*, **218**, e20201811.

Su, M.T., Inui, M., Wong, Y.L., Takahashi, M., Sugahara-Tobinai, A., Ono, K., Miyamoto, S., Murakami, K., Itoh-Nakadai, A., Kezuka, D., Itoi, S., Endo, S., Hirayasu, K., Arase, H. & Takai, T. (2021) Blockade of checkpoint ILT3/LILRB4/gp49B binding to fibronectin ameliorates autoimmune disease in BXSB/Yaa mice. *Int. Immunol.*, **33**, 447-458.

Su, M.T., Kumata, S., Endo, S., Okada, Y. & Takai, T. (2022) LILRB4 promotes tumor metastasis by regulating MDSCs and inhibiting miR-1 family miRNAs. *Oncoimmunology*, **11**, 2060907.

Takahashi, N., Itoi, S., Su, M.T., Endo, S. & Takai, T. (2022) Co-localization of fibronectin receptors LILRB4/gp49B and integrin on dendritic cell surface. *Tohoku J. Exp. Med.*, **257**, 171-180.

Turner, H. & Kinet, J.P. (1999) Signalling through the high-affinity IgE receptor Fc epsilonRI. *Nature*, **402**, B24-30.

van Vugt, M.J., Heijnen, I.A., Capel, P.J., Park, S.Y., Ra, C., Saito, T., Verbeek, J.S. & van de Winkel, J.G. (1996) FcR gamma-chain is essential for both surface expression and function of human Fc gamma RI (CD64) in vivo. *Blood*, **87**, 3593-3599.

Wang, L.L., Chu, D.T., Dokun, A.O. & Yokoyama, W.M. (2000) Inducible expression of the gp49B inhibitory receptor on NK cells. *J. Immunol.*, **164**, 5215-5220.

Wang, L.L., Mehta, I.K., LeBlanc, P.A. & Yokoyama, W.M. (1997) Mouse natural killer cells express gp49B1, a structural homologue of human killer inhibitory receptors. *J. Immunol.*, **158**,

13-17.
Wong, Y.L., Su, M.T., Sugahara-Tobinai, A., Itoi, S., Kezuka, D., Endo, S., Inui, M. & Takai, T. (2019) Gp49B is a pathogenic marker for auto-antibody-producing plasma cells in lupus-prone BXSB/Yaa mice. *Int. Immunol.*, **31**, 397-406.
Xu, Z., Chang, C.C., Li, M., Zhang, Q.Y., Vasilescu, E.M., D'Agati, V., Floratos, A., Vlad, G. & Suciu-Foca, N. (2018) ILT3.Fc-CD166 interaction induces inactivation of p70 S6 kinase and inhibits tumor cell growth. *J. Immunol.*, **200**, 1207-1219.
Zhou, J.S., Friend, D.S., Feldweg, A.M., Daheshia, M., Li, L., Austen, K.F. & Katz, H.R. (2003) Prevention of lipopolysaccharide-induced microangiopathy by gp49B1: evidence for an important role for gp49B1 expression on neutrophils. *J. Exp. Med.*, **198**, 1243-1251.
Zhou, J.S., Friend, D.S., Lee, D.M., Li, L., Austen, K.F. & Katz, H.R. (2005) gp49B1 deficiency is associated with increases in cytokine and chemokine production and severity of proliferative synovitis induced by anti-type II collagen mAb. *Eur. J. Immunol.*, **35**, 1530-1538.